Journal of Nanobiotechnology

RESEARCH

Open Access

Enzyme/ROS dual-sensitive nanoplatform with on-demand Celastrol release capacity for enhanced ulcerative colitis therapy by ROS scavenging, microbiota rebalancing, inflammation alleviating

Jinfeng Shi[1], Jiahui Zhou[1], Bo Liu[1], Kezhou Lin[1], Xingliang Xie[1], Xue Han[1], Yanmei Sheng[1], Yihan Liu[1], Congjian He[1], Yujin Zhou[1], Nan Zhu[1], Qian Yang[1], Ruifeng Luo[2*] and Yi Li[1*]

Abstract

Background The oral administration of drugs for treating ulcerative colitis (UC) is hindered by several factors, including inadequate gastrointestinal stability, insufficient accumulation in colonic lesions, and uncontrolled drug release.

Methods A multiple sensitive nano-delivery system comprising β-cyclodextrin (CD) and 4-(hydroxymethyl) phenylboronic acid (PAPE) with enzyme/reactive oxygen species (ROS) sensitivity was developed to load celastrol (Cel) as a comprehensive treatment for UC.

Results Owing to the positive charge in the site of inflamed colonic mucosa, the negatively charged nanomedicine (Cel/NPs) could efficiently accumulate. Expectedly, Cel/NPs showed excellent localization ability to colon in vitro and in vivo tests. The elevated concentration of ROS and intestinal enzymes in the colon microenvironment quickly break the CD, resulting in Cel release partially to rebalance microbiota and recover the intestinal barrier. The accompanying cellular internalization of residual Cel/NPs, along with the high concentration of cellular ROS to trigger Cel burst release, could decrease the expression of inflammatory cytokines, inhibit colonic cell apoptosis, promote the macrophage polarization, scavenge ROS, and regulate the TLR4/NF-κB signaling pathway, which certified that Cel/NPs possessed a notably anti-UC therapy outcome.

Conclusions We provide a promising strategy for addressing UC symptoms *via* an enzyme/ROS-sensitive oral platform capable of releasing drugs on demand.

Keywords Enzyme/ROS-triggered controlled release, Ulcerative colitis, Celastrol, ROS scavengers

*Correspondence:
Ruifeng Luo
ruifengluo128@163.com
Yi Li
liyichengdu29@126.com

Full list of author information is available at the end of the article

Graphical Abstract

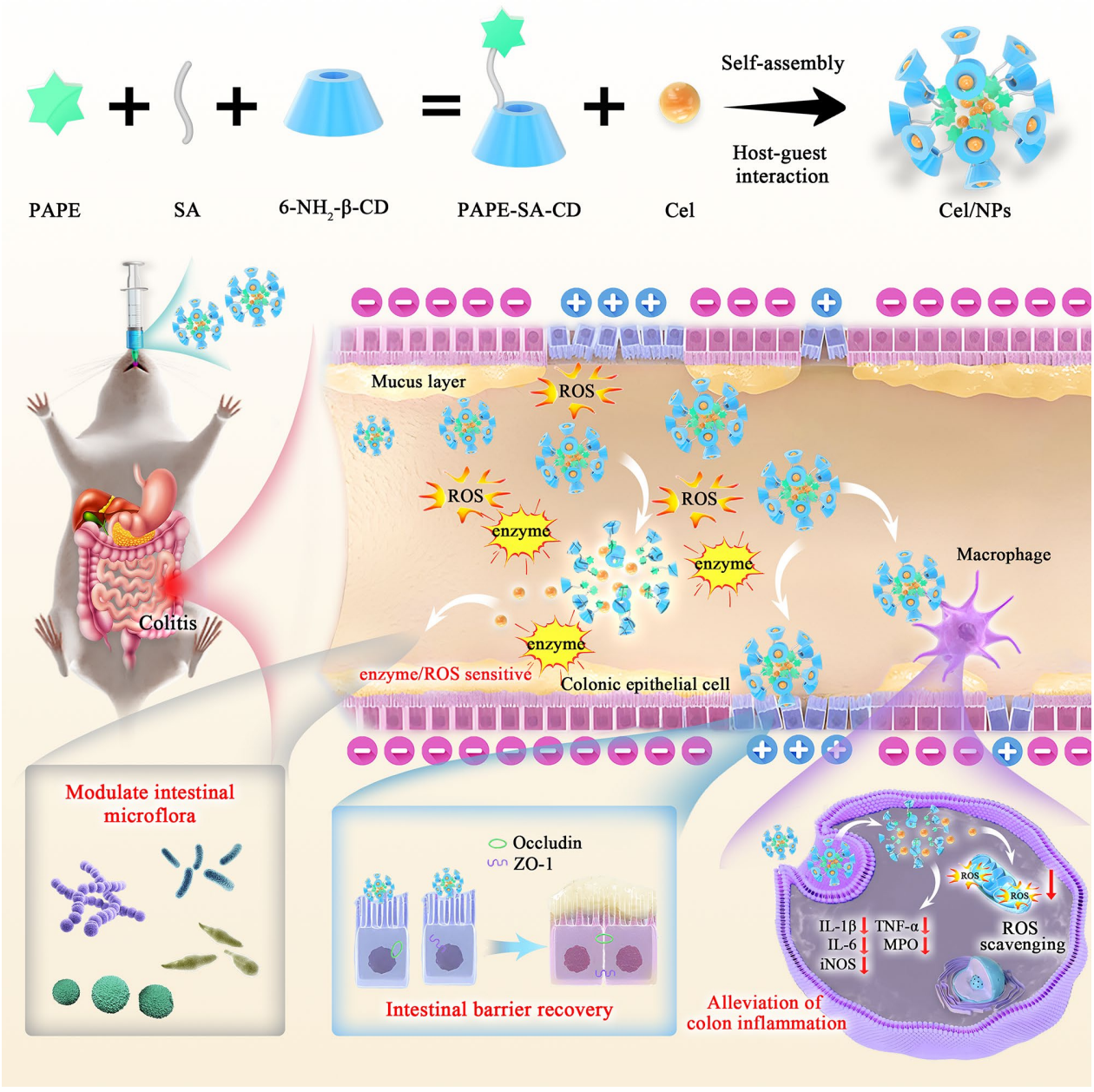

Introduction

Ulcerative colitis (UC) is a common chronic and recurrent inflammatory disease associated with mucosal ulcers, colon bleeding, diarrhea, as well as abdominal pain [1]. According to reports, the high recurrence rates and lifelong care requirements associated with UC significantly impact the quality of life for 7 million people globally [2]. Therapeutic strategies thus focus on achieving and maintaining remission from inflammatory episodes. Disease severity is generally categorized into mild and moderate to severe based on clinical symptoms, laboratory values, biomarkers, and endoscopic findings (1–3) [3]. Currently, mesalamine and sulfasalazine are the first-line treatments for inducing remission in mild-to-moderate UC, but they often cause adverse effects due to their non-specific anti-inflammatory properties. Although small-molecule Janus kinase (JAK) inhibitor tofacitinib and biologics are commonly used to treat moderate-to-severe UC, they are significantly limited by high costs and increased drug resistance [4, 5]. Acute-severe UC necessitates hospitalization due to its life-threatening nature. For patients with this type of

UC undergoing hospital treatment, cyclosporine, steroids, and infliximab are the currently accepted medical therapies [6]. While these medications can mitigate inflammation to a certain degree, 30 to 50% of patients still experience minimal to no improvement. Moreover, prolonged administration heightens the risk of relapse and numerous adverse effects, thereby constraining their broader clinical utility [7]. Hence, there is an immediate imperative to devise novel treatment approaches aimed at improving targeting efficacy and minimizing side effects. Currently, there is mounting interest in exploring the therapeutic efficacy of natural anti-inflammatory phytochemicals in managing UC. These compounds are under scrutiny as potential alternative therapies for patients exhibiting inadequate response to conventional medications.

Celastrol (Cel), derived from *Tripterygium wilfordii* Hook F, is regarded as one of the top five promising bioactive compounds in nature [8, 9]. Interestingly, Cel demonstrated a variety of excellent bioactivities in treating numerous inflammatory-related diseases, including atherosclerosis, obesity, arthritis, liver fibrosis, inflammatory bowel disease, etc. [10–14]. Of these, Cel has shown promise in alleviating UC by modulating oxidative stress, inflammatory cytokines, and intestinal homeostasis [15, 16]. Nevertheless, the hydrophobicity and finite colonic targeting of Cel severely limit its clinical application [10]. Currently, the development of Cel-derived structural derivatives and nano/microcarrier systems have been extensively employed to ameliorate the solubility and deliverability [17]. Nonetheless, it is essential to note that certain challenges remain in the treatment of UC utilizing these strategies, including utilizing harmful chemicals, complicated preparation of materials, resisting the destruction of drugs by the stomach and small intestine, and effectively delivering drugs to the inflammatory site of UC.

In recent years, a new class of stimuli-responsive nanoplatforms has emerged, designed specifically for drug delivery, which can modulate encapsulated drugs release *via* the particular physicochemical properties of colon tissue, including acidic pH conditions [18, 19], overproduction of reactive oxygen species (ROS) [20], internal enzymes in colon [21, 22]. β-Cyclodextrin (CD) belongs to natural cyclic oligosaccharides consisting of α-1,4-glucoside bonds with cone-like structures, which demonstrate numerous advantages including accessibility, less toxicity, excellent biocompatibility and low cost [23]. More essentially, it displays a hydrophilic surface externally, while internally it features a relatively hydrophobic cavity [24]. As a result of colonic microbial fermentation and enzymatic hydrolysis, CD rings can be opened, and subsequently, ester bond hydrolysis occurs, leading to drug release in the colon [21]. Nonetheless, some drawbacks of CD need to be taken care of, taking into account the effects of dilution and competitive inclusion, the inclusion complexes derived from CD generated through non-covalent bonds are readily exposed to gastrointestinal fluids prior to reaching the colon. This results in early drug release. Researchers have endeavored to covalently link CD with drugs or chemically bond environment-responsive molecules, aiming to regulate drug release in the colon [25].

Hence, our study constructed an oral Cel encapsulated nano platform with dual enzyme/ROS sensitivity and excellent adhesion ability for UC treatment. 4-(hydroxymethyl) phenylboronic acid pinacol ester (PAPE) was covalently linked with CD to form an enzyme/ROS-sensitive material (PAPE-SA-CD), following that encapsulated Cel via the amphiphilic nature of the obtained PAPE-SA-CD in combination with host-guest interaction (Scheme 1). Initially, leveraging the negative charge of Cel/NPs, celastrol can be selectively transported to inflamed sites in the colon through electrostatic attraction. Secondly, based on the high concentration of ROS and intestinal enzymes in the colon, Cel can be localized to the inflamed site to minimize systemic exposure and adverse effects. For the purpose of verifying this hypothesis, a thorough investigation of the physicochemical properties and pharmacological efficacy of Cel/NPs in vitro and in vivo was conducted. Additionally, we investigated the gastrointestinal stabilization of Cel/NPs to emphasize the enzyme/ROS sensitivity of Cel/NPs. Besides, the anti-DSS-induced inflammation effects are researched via TLR4/NF-κB signaling pathway regulation, intestinal barrier recovery, and intestinal microflora modulation in vivo. In conclusion, our findings indicate that CD in conjunction with PAPE has the potential to be developed as a promising treatment platform for UC via oral administration.

Methods

Materials

Cel was obtained from Chengdu DeSiTe Biological Technology Co., Ltd. (Chengdu, China). 4-(hydroxymethyl) phenylboronic acid (PAPE), 4-dimethylamino pyridine (DAMP), N-Hydroxysuccinimide (NHS), 1-(3-dimethyl aminopropyl)-3-ethyl carbodiimide hydrochloride (EDC), Tetrahydrofuran (THF), Succine anhydride (SA), Triethylamine (TEA), Dimethyl sulfoxide (DMSO), and Coumarin-6 (C6) were originated from Aladdin Reagent Co., Ltd (Shanghai, China). Mono-(6-amino-6-deoxy)-beta-cyclodextrin (6-NH_2-β-CD) was provided by Shandong Binzhou Zhiyuan Biotechnology Co., Ltd. (Shandong, China). 4,6-diamidino-2-phenylindole (DAPI) was acquired from Wuhan Service-bio Technology Co., Ltd. (Wuhan, China). ROS Assay Kit based on 20, 70-dichlorofluorescein diacetate (DCFH-DA) was

purchased from Suzhou Yuheng Biotechnology Co., Ltd. (Suzhou, China). Besides, the near-infrared lipophilic carbocyanine dye 1,10-di octadecyl tetramethyl indotricarbocyanine iodide (DiR) originated from Mellon, Biological Technology Co., Ltd. (Dalian, China). Moreover, the mouse interleukin-1β(IL-1β) ELISA kit, the mouse TNF-α ELISA kit, the mouse interleukin-6 (IL-6) ELISA kit and the myeloperoxidase (MPO) ELISA kit were supplied by Multi-Science (Lianke) Biotech Co., Ltd. (Hangzhou, China). Except for that, the inducible nitric oxide synthase (iNOS) assay kit was purchased from Elabscience Biotechnology Co., Ltd. (Wuhan, China). Anti-TLR4 antibody, anti-MYD88 antibody, and anti-NF-κB p65 antibody were supplied by Wuhan Service-bio Technology Co., Ltd. (Wuhan, China). Meanwhile, dextran sodium sulfate (DSS, MW = 36–50 kDa) was purchased from MP Biomedicals Inc. (Irvine, CA, USA). NCM 460 cells and RAW 264.7 cells were acquired from Guangzhou Saiku Biotechnology Co., Ltd. (Guangzhou, China). Male ICR mice (4 weeks old) were purchased from SPF (Beijing) Biotechnology Co., Ltd. (Beijing, China). The animal-related experiments gained approval from the Animal Ethics Committee of Chengdu Medical College.

Synthesis and characterization of PAPE-SA-CD

PAPE-SA was synthesized referring to the previous method [26]. Detailed steps can be found in supplementary materials.

The synthesis of PAPE-SA-CD polymer utilizing amide reaction. It was conducted by accurately weighing PAPE-SA (2.13 mmol) and subsequently dissolving in 15 mL of anhydrous DMSO, sequentially adding NHS (4 mmol), EDC·HCl (4 mmol) and triethylamine (TEA) (4 mmol) at 25˚C for 3 h, during which nitrogen gas was continuously introduced. 6-NH_2-β-CD (2.13 mmol) was aforementioned reaction system was supplemented for 48 h. The impurities in the reaction solution were removed employing the dialysis method (with a molecular weight of 1200 Da in the dialysis bag), and deionized water was adopted as the dialysis solution for 3 d. The ultimate outcome of freeze-drying resulted in the powdered PAPE-SA-CD polymer.

^{1}H NMR spectra of PAPE-SA and PAPE-SA-CD were acquired on a Bruker instrument (AVANCE NEO 700 MHz spectrometer, Bruker, Germany). Besides, FTIR spectra of PAPE-SA and PAPE-SA-CD were characterized by an IR instrument (IR Tracer-100, Shimadzu, Kyoto, Japan).

Preparation and characterization of Cel/NPs

Cel/NPs were constructed employing the nano-precipitation method. In detail, Cel (2 mg) and PAPE-SA-CD (25 mg) were dissolved in DMSO (2 mL). Subsequently, the mixture was introduced gradually into a 10 mL aqueous solution and agitated for a duration of 2 h. Subsequent to this, a dialysis bag with a molecular weight cutoff of 3000 (manufactured by Millipore) was employed for the dialysis process in deionized water, spanning a period of 12 h, thereby yielding a dispersion of Cel/NPs. A syringe filter (0.45 μm) was introduced to remove free Cel and store the above solution at 4 °C.

Dynamic light scattering (DLS) with a Nanosizer ZS90 (Malvern, UK) was used to measure the hydrodynamic diameters (nm), polydispersity index (PDI) and zeta potential (mV) of Cel/NPs. A transmission electron microscope (TEM, JEM 1200X, JEOL, Japan) was employed to evaluate the morphology of Cel/NPs. Additionally, we measured the X-ray powder diffraction (XRD) spectra of Cel, Blank NPs, Cel/NPs and the physical mixture between Cel and all polymers on an XRD diffractometer (D8 Advance, BRUKER, Germany) in the range of 5 ° to 90 °. Additionally, a 7-day observation of Cel/NPs was conducted by measuring their hydrodynamic diameters, PDI, and zeta potentials to verify their stability. [27].

The HPLC was subsequently performed to analyze the encapsulation efficiency (EE) and loading efficiency (LE) of Cel/NPs to Cel. The formula employed to determine EE and LE is as follows:

$$EE\ (\%) = m_{drug\ in\ NPs}/m_{total\ drug} \times 100\%.$$

$$LE\ (\%) = m_{drug\ in\ NPs}/m_{total\ mass\ of\ NPs} \times 100\%.$$

ROS/enzyme dual-sensitive and release profiles of Cel/NPs

ROS/enzyme sensitivity investigation of Cel/NPs

The oxidation- and/or enzyme-sensitive properties of Cel/NPs were researched under distinct conditions. Cel/NPs were incubated in 1 mM H_2O_2 and 10 IU/mL α-amylase solutions and subsequently shaken with the speed of 100 rpm at 37℃ for 24 h, respectively [21, 28]. After incubation, the average particle diameters of Cel/NPs were measured using DLS, and their morphologies were examined via TEM.

Drug release evaluation in vitro

A dialysis method was employed to determine Cel release profiles in Cel/NPs [29]. Briefly, free Cel, CD-Cel, and Cel/NPs were successively dispersed within simulated stimulation fluid from gastric (0–2 h in SGF) to small intestine (2–6 h in SIF) to colon (6–48 h in SCF). Next, adding Tween-80 (0.5% w/v) to the releasing medium facilitated Cel dissolution. Meanwhile, 3 mL of the samples was injected into a separate dialysis bag (MWCO 3000, Millipore). At predetermined intervals, 1 mL of the simulated solution was withdrawn and replaced with an equivalent volume of fresh simulated solution. The Cel concentration in the resulting filtrate was measured by HPLC as previously described. Each sample was tested in triplicate.

3 mL of Cel/NPs were fed into the dialysis bags (MWCO 3000, Millipore) and subsequently incubated with or without 1 mM H_2O_2 and 10 IU/mL α-amylase in pH 7.4 PBS (containing 0.5% (w/v) Tween-80) for 48 h at 37℃ to examine Cel release properties of PAPE-SA-CD-based-NPs in the colon.

Intracellular uptake of Cel/NPs

A pivotal part of nano-drug evaluation in vitro is cellular uptake. During this study, NCM 460 cells (colonic epithelial cells) and Raw 264.7 cells (inflammatory-associated cells) were chosen to test the ability of cellular internalization of drugs. Moreover, C6 (a hydrophobic fluorescence probe) was substituted for Cel to prepare free C6, CD-C6, and C6/NPs. Confocal laser scanning microscopy (CLSM; Nikon A1R+SIM; Nikon, Tokyo, Japan) was employed to analyze cellular uptake qualitatively. NCM 460 cells or Raw 264.7 cells were cultured in confocal dishes and incubated for 12 h. Following this incubation, the cells were treated with various preparations (free C6, CD-C6, and C6/NPs, each containing 100 ng/mL of C6) for 4 h. The cells were then washed three times with cold PBS, fixed with 4% paraformaldehyde solution, and stained with DAPI. Finally, the cells were observed using CLSM.

In addition, flow cytometry (FCM; NovoCyte; ACEA, San Diego, CA) was employed to analyze cellular uptake quantitatively. Initially, NCM 460 cells or Raw 264.7 cells were cultured in 12-well plates for 12 h. For the time-dependent study, C6/NPs (C6 concentrations of 100 ng/mL) were incubated with cells for 0.25, 0.5, 1, 2, and 4 h, respectively. For a concentrations-dependent study, the cells were treated with different C6/NPs concentrations (C6 concentrations of 25, 50, 100, 150, and 200 ng/mL) for 4 h. Moreover, the cells were separately treated with various Cel preparations (free C6, CD-C6, and C6/NPs, C6 content of 100 ng/mL) for 4 h to confirm the distinctions in cellular uptake ability. Finally, after three washes with cold PBS, the cells were centrifuged and resuspended in PBS for FCM analysis.

ROS scavenging, anti-apoptosis and macrophage polarization activities of Cel/NPs

Raw264.7 or NCM460 cells were treated with free Cel, CD-Cel, and Cel/NPs (Cel content is 0.5 μg/mL), and mixed with lipopolysaccharide (LPS) (1 μg/mL), respectively [30]. The cells of the control group remained untreated and the model group grown in a medium supplemented with LPS only. Besides, the DCFH-DA assay was employed to determine ROS production in Raw264.7 and NCM460 cells, and all samples were observed by CLSM (Nikon A1R+SIM; Nikon, Tokyo, Japan).

Moreover, the anti-apoptotic activity of Cel/NPs was evaluated using FCM. In detail, NCM460 cells were cultivated with free Cel, CD-Cel, and Cel/NPs (Cel content is 0.5 μg/mL) for 24 h. In the following, the cells were processed into single-cell suspensions and subsequently stained by Annexin V-Alexa Fluor488/PI. Finally, the cells were collected for FCM analysis (NovoCyte; ACEA, San Diego, CA).

An LPS-stimulated (1 μg/mL) conversion into M1 type was conducted in Raw264.7 cells to verify Cel/NPs' polarizing effects on macrophages. Subsequently, LPS-induced macrophages were co-cultured with different Cel-loaded preparations (free Cel, CD-Cel, and Cel/NPs, Cel content is 0.5 μg/mL). CD86 and CD206 macrophage markers were quantified in M1 macrophages via FCM.

Biodistribution evaluation and target properties of Cel/NPs in vivo

The localization and biodistribution of Cel/NPs were studied in UC model mice (induced with 3% DSS) following oral administration. Besideds, the fluorescence probe of DiR was used to instead of Cel. UC model mice were given different DiR-loaded preparations (the concentration of DiR is 3 mg/kg), including free DiR, CD-DiR, and DiR/NPs, respectively [31]. At predetermined intervals, photos were taken with the Caliper Life Sciences LIVIS® Lumina Series (PerkinElmer, Waltham, MA, USA). Finally, the mice were euthanized 24 h after administration, and their colons were excised and photographed. The intensity of localized fluorescence was quantified using in vivo imaging software.

We further examined the targeted properties of inflammation of Cel/NPs in vivo. The UC mice were treated with free C6, CD-C6, and C6/NPs (the concentration of C6 is 5 mg/kg), respectively. Following 12 h of oral administration, the colon was collected, cut into slices and stained with DAPI. Finally, the fluorescence of the colon was captured using CLSM.

Therapeutic effectiveness of Cel/NPs in vivo

UC mouse model was established by freely drinking DSS solution (3%, w/v) for 7 d and randomly divided into four groups (model, free Cel, CD-Cel and Cel/NPs; $n=6$ per group). Moreover, the mice of control group were freely drunk water, and the mice of free Cel group, CD-Cel group and Cel/NPs group were treated with various preparations of Cel at 3 mg/kg/d orally from day 3 to day 10. The control group and model group received saline only.

Throughout the experiment, a comprehensive assessment of the mice's daily weight and disease activity index (DAI) was conducted. Upon conclusion of the experiment, blood samples, as well as the colon and major organs (heart, liver, spleen, lung, and kidney) of the mice, were collected. Additionally, we recorded the status of the colon and measured the length, as well as weighed

the weight of the spleen. Besides, the colon tissues were conducted hematoxylin/eosin (H&E) and periodic acid schiff (PAS) staining, separately. Additionally, the levels of cytokines (IL-1β, IL-6 and TNF-α) in the colon were determined by ELISA kits, and the levels of MPO and iNOS were detected via a commercially available MPO kit and iNOS kit, respectively. Meanwhile, the expression level of occluding and ZO-1 in the colon were detected by immunofluorescence staining and pictured via a Pannoramic ScanII (3DHISTECH, Budapest, Hungary). The expression of MYD88, NF-κB p65, and TLR4 in the colon was detected by immunohistochemical staining and captured via a fluorescence microscope (Nikon Eclipse Ci, Tokyo, Japan). The intensity of fluorescence was quantified using ImageJ software. Blood biochemistry analysis, including measurements of hepatotoxicity indicators ALT and AST, as well as nephrotoxicity indicators BUN and CRE, along with examination of organ pathological sections, were conducted to evaluate the safety profile of Cel/NPs.

16 S rRNA gene sequencing analysis

Collection of fecal samples and extraction of total fecal DNA were employed for 16 S rRNA gene sequencing analysis. Besides, the PCR amplification was in the V3-V4 hypervariable region of 16 S rDNA [32]. In the following, α diversity analysis, PCoA, Venn diagram analysis, and the species abundance and composition of the bacterial community were conducted in different groups.

Statistical analysis

All data are presented as mean ± SD. Statistical significance was determined using Student's t-test or one-way analysis of variance (ANOVA). Significance levels were denoted as $^{*}P<0.05$, $^{**}P<0.01$, and $^{***}P<0.001$.

Results

Characterization of intermediate and final products

The two-step reactions were adopted to synthesize PAPE-SA-CD, as depicted in Fig. 1A. ^{1}H NMR and FTIR were employed to elucidate the structures of PAPE, SA, PAPE-SA, CD, and PAPE-SA-CD. Besides, the characteristic proton peak assignments were displayed in Fig. 1B [28]. The signals at 2.50 ppm were ascribed to deuterium DMSO. The characteristic peaks at 7.76 ppm (a) and 7.30 ppm (b) belonged to the aromatic region, which suggests successful binding of PAPE. Besides, the signal resonances in the protons of the sugar ring in 6-NH_2-β-CD at 5.68–5.84 ppm (c), thus illustrating that 6-NH_2-β-CD is well conjugated to PAPE-SA-CD. In the FTIR spectra (Fig. 1C), PAPE-SA-CD displayed the stretching vibration associated with the B-O bond at 1327 cm^{-1}, demonstrating PAPE was connected successfully. Moreover, PAPE-SA-CD exhibited the amide II absorption band (bending vibration of N-H bonds) in its spectrum at 1650 cm^{-1}, thus implying that 6-NH_2-β-CD is well conjugated to PAPE-SA.

Characterization of Cel/NPs

A single step is involved in preparing Cel-encapsulated oral drug delivery systems [33]. Cel/NPs were prepared using the nanoprecipitation method based on the amphiphilic nature of the obtained PAPE-SA-CD combined with host-guest complexes. It was characterized using size distribution, PDI, zeta potential, EE, LE, TEM, and XRD. According to the results, the particle size and PDI of Cel/NPs are approximately 50.04 ± 0.74 nm, 0.139 ± 0.046, respectively (Fig. 2A). The zeta potential of Cel/NPs is about −16.1 ± 0.6 mV (Fig. 2B). The entrapment efficiency is high, with EE and LE reaching 91.08 ± 2.31% and 6.75 ± 0.06%, respectively (Figure S1). Besides, it was documented that Cel/NPs have a uniform spherical structure by TEM images (Fig. 2E). Hence, Cel/NPs contain controllable drug loading and a particle size suitable for delivering Cel. Additionally, as illustrated in Figure S1, a single β-CD is inefficient in encapsulating Cel (The EE is 65.18 ± 1.77%), which indicates that the join of PAPE contributes substantially to the loading of NPs. The aforementioned results demonstrate that Cel/NPs are spherical nanoparticles with a uniform particle size and high entrapment efficiency.

XRD spectra were investigated to gain a better understanding of the molecular interaction between the drug and the carrier, which affects the drug release characteristics. In Fig. 2C, the XRD pattern of free Cel demonstrates numerous sharp peaks between 5 ° and 90 °, indicating high crystallinity. Besides, the lack of these peaks in Cel/NPs suggests that no crystal complex exists between Cel and PAPE-SA-CD matrix. Consequently, Cel exists as an amorphous or disordered crystal.

Stability evaluation of Cel/NPs

Additionally, Cel/NPs were placed at 4℃ for 7 d to evaluate their stability. Based on the 7-day test results (Fig. 2D and Figure S2), the size of Cel/NPs kept little change, which indicating its relatively stable. Additionally, a stable trend was observed in the PDI and zeta potential of Cel/NPs over 7 d.

ROS- and enzyme-responsive capabilities of Cel/NPs

To verify the sensitivity of Cel/NPs to ROS or α-amylase, the size distribution and morphological changes of Cel/NPs were measured by DLS and TEM in distinct simulated environments for 24 h, respectively. Figure 2E illustrates that there is an increase in the particle size of Cel/NPs and even appears heterogenous peaks on the condition that incubating with 1 mM H_2O_2 or 10 IU/mL α-amylase for 24 h. Further evidence from TEM revealed

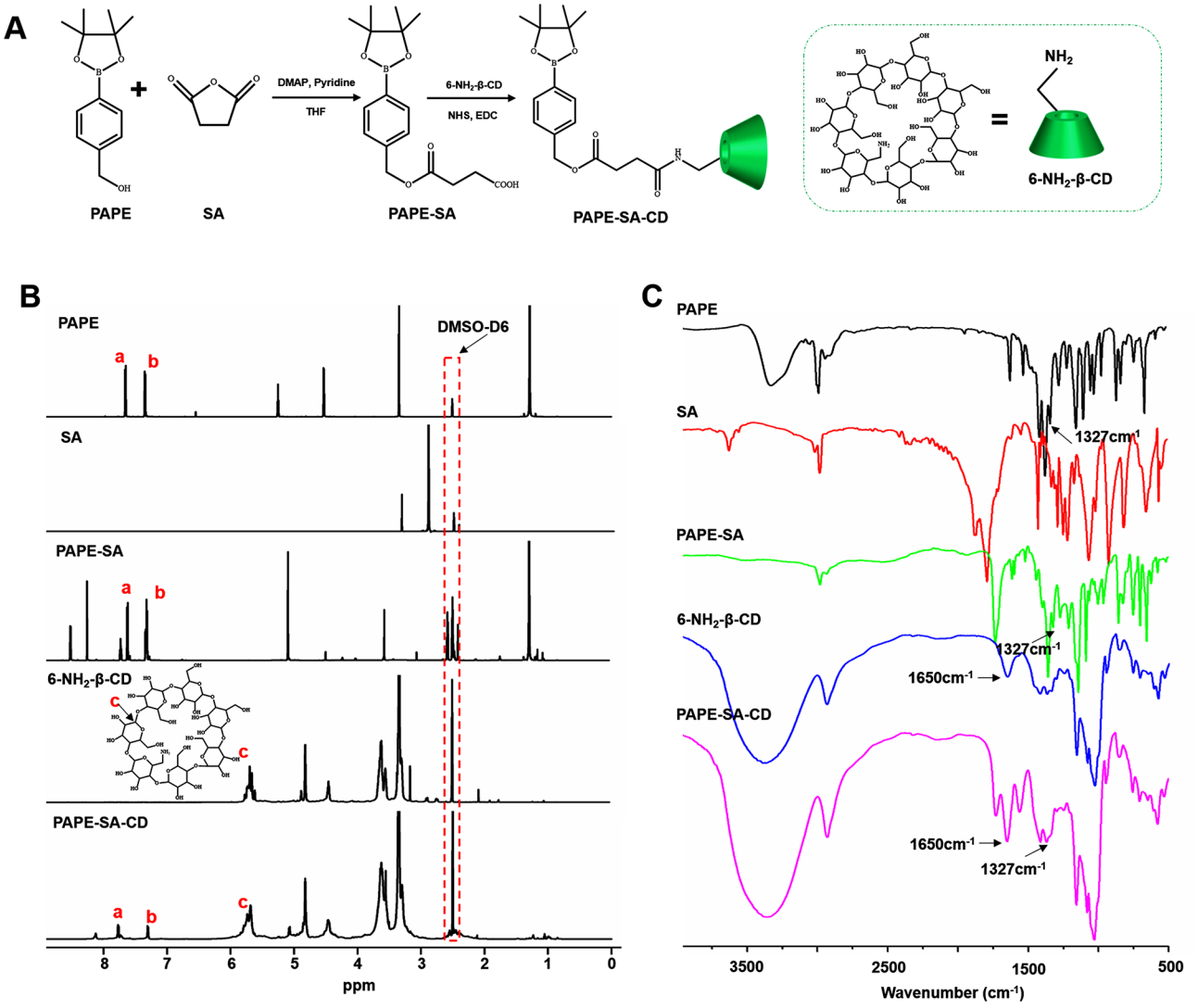

Fig. 1 Copolymer synthesis and characterization. (**A**) Synthesis route of PAPE-SA-CD. (**B**) ^{1}H NMR spectrogram of PAPE-SA-CD. (**C**) FTIR spectrogram of PAPE-SA-CD

that the presence of H_2O_2 or α-amylase could cause the surface of Cel/NPs to become irregular (Fig. 2E). These results are attributed to ROS sensitivity caused by the breakage of PAPE with H_2O_2 and enzyme sensitivity result in the β-CD under α-amylase. Moreover, the single sensitivity of Cel/NPs to reactive oxygen or α-amylase is predicted by the above results. Further research is needed to confirm the dual sensitivity of Cel/NPs in evaluating their release behavior.

Release profiles of Cel/NPs

The Cel release contents from free Cel, CD-Cel, or Cel/NPs were measured in the whole GI tract (Place in the alternative medium continuously). According to Fig. 2F, free Cel was released quickly into SGF and SIF, and the cumulative release rate was 58.84% at 6 h. After Cel was encapsulated, both CD-Cel and Cel/NPs exhibited a slower Cel release characteristic. The cumulative release rate for CD-Cel and Cel/NPs was only 7.03% and 5.48% at 6 h, respectively. Moreover, after 48 h, Cel/NPs also almost released minor drugs, with a 39.81% cumulative release rate. Consequently, due to the biodegradable nature of PAPE-SA-CD, Cel/NPs could reach the colon tissue from the stomach and small intestine.

Furthermore, a simulation of drug release behavior at the colitis site was conducted using ROS and enzyme stimulators in a synergistic partnership. The controlled release curves of Cel/NPs are investigated including pH 7.4 buffer, pH 7.4 buffer with 1 mM H_2O_2, pH 7.4 buffer with 10 IU/mL α-amylase and pH 7.4 buffer with 1 mM H_2O_2 and 10 IU/mL α-amylase (Fig. 2G). In the presence of H_2O_2 or α-amylase, the results indicated that the drug release rate was significantly accelerated, reaching cumulative release rates of 70.77% and 75.34% at 6 h,

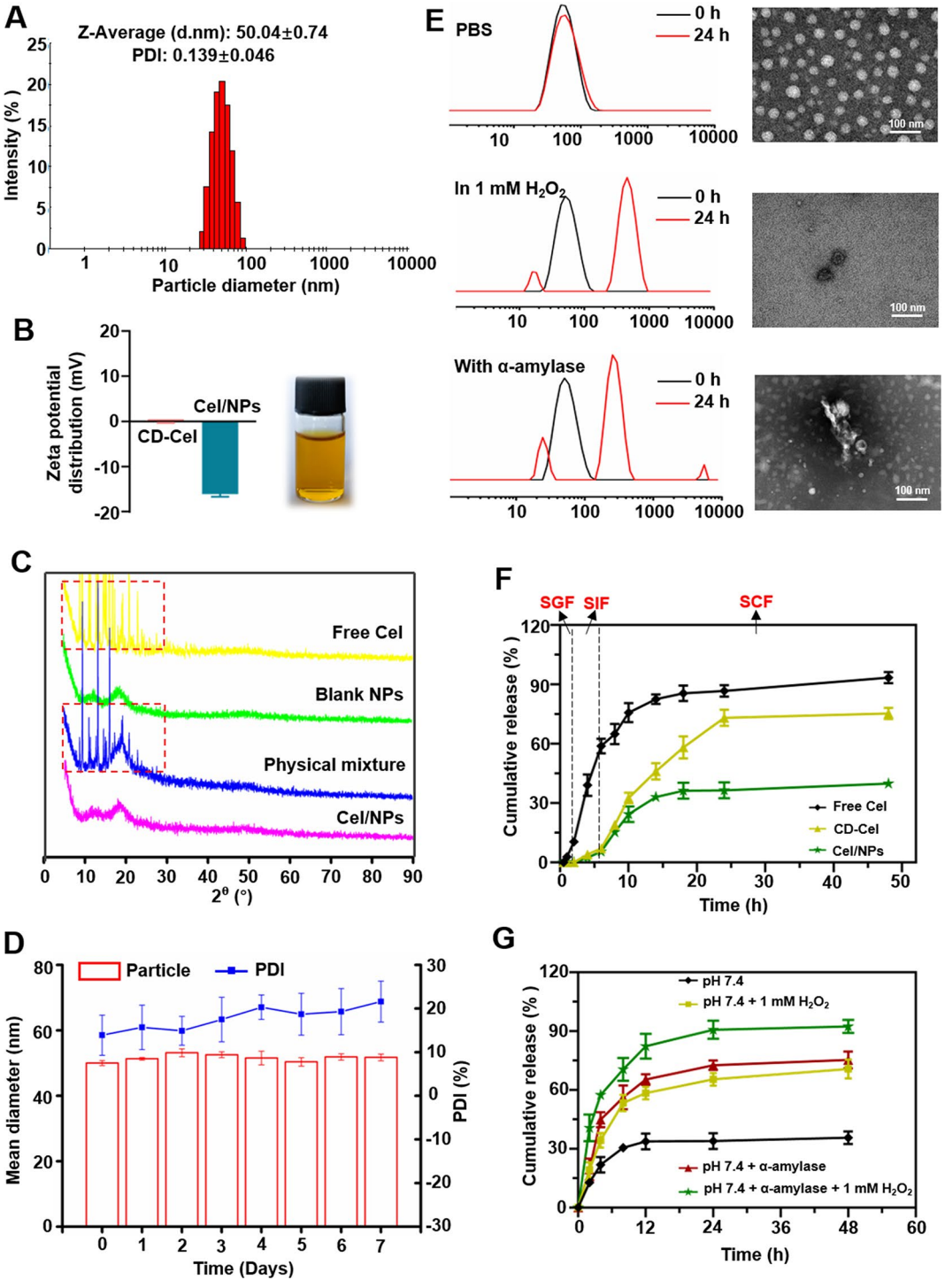

Fig. 2 Characterization of Cel/NPs. (**A**) Average particle size and PDI of Cel/NPs. (**B**) Zeta potential of Cel/NPs. (**C**) XRD analysis. (**D**) Mean diameter and PDI results of Cel/NPs within 7 d. (**E**) Size distribution and TEM image of Cel/NPs in different conditions. (**F**) Release profiles of free Cel, CD-Cel and Cel/NPs in SGF, SIF, SCF ($n = 3$). (**G**) Release profiles of Cel/NPs with or without 1 mM H_2O_2 or 10 IU/mL α-amylase within 48 h ($n = 3$)

respectively. Additionally, in a pH 7.4 buffer containing 1 mM H_2O_2 and 10 IU/mL α-amylase, a total of 92.50% of Cel was released within 48 h. This may be due to the oxidation of PAPE and the enzyme-responsive nature of CD. Based on these results, controlled drug release was achieved by internally stimulating ROS/enzyme with Cel/NPs.

In vitro cell internalization profiles of Cel/NPs

Effective cellular uptake is a prerequisite for Cel/NPs to exert anti-UC effects. In this study, two types of cells associated with the colon (NCM460 and Raw264.7) were examined for Cel/NPs uptake, and Cel/NPs were labeled using the fluorescent probe C6 encapsulated within NPs. Besides, a qualitative and a quantitative analysis of the cell internalization profiles of C6/NPs was examined via CLSM and FCM. The results from Fig. 3A, E demonstrate that NCM460 cells and Raw264.7 cells treated with CD-C6 or C6/NPs for 4 h demonstrated more obvious green fluorescence than free C6. Interestingly, both NCM460 cells and Raw264.7 cells exposed to C6/NPs exhibited stronger fluorescence compared to those exposed to CD-C6, indicating the greater capacity of PAPE-SA-CD to enhance drug internalization in cells.

Furthermore, drug internalization in cells was quantitatively analyzed using FCM. According to Fig. 3B, F, as time increases, the fluorescence intensity within both NCM460 cells and Raw264.7 cells likewise increases, which indicates that the cell uptake of C6/NPs is time-dependent. Besides, on the condition that C6 concentrations increase from 25 to 200 ng/mL, the intracellular fluorescence intensity also indicates an increasing trend, demonstrating the cellular uptakes of NCM460 cells and Raw264.7 cells were dose-dependent (Fig. 3C, G). Next, as shown in Fig. 3D, H, on the condition that NCM460 cells and Raw264.7 cells were treated with distinct C6 preparations for 4 h, the C6/NPs group exhibited significantly higher fluorescence intensity than free C6 or CD-C6 groups. Therefore, the findings from FCM align with those obtained from CLSM, indicating that the cellular absorption capability of C6/NPs surpassed that of free C6 and CD-C6, which may be attributed to the efficient encapsulation of PAPE-SA-CD polymer.

In vitro ROS scavenging, anti-apoptosis and macrophage polarization activities

Inflammation is driven by abnormal ROS generation [34]. Thus, our study focused on whether Cel/NPs could inhibit ROS production in NCM460 cells and Raw264.7 cells. As illustrated in Fig. 4A, B, following 24 h of stimulation with LPS (1 μg/mL), the two type cells produced a large amount of ROS, which was probed by the fluorescent dye 2′,7′-dichlorofluorescein-diacetate (DCFH-DA). Nonetheless, following incubation with distinct Cel preparations (Cel content of 0.5 μg/mL) for 24 h [15], the fluorescence intensity of DCFH-DA was noticeably weaker in comparison with the model group, in the special Cel/NPs group. Notably, the ability of Cel/NPs to ROS exceeded that of CD-Cel or free Cel in both NCM460 cells and Raw264.7 cells. This supports the therapeutic potential of Cel/NPs in in vivo models of UC.

The prolonged buildup of ROS is a characteristic feature of UC. Therefore, implementing measures to eliminate ROS could inhibit apoptosis in colon cells. To further elucidate the cellular protective effects, the apoptosis of NCM460 cells treated with various formulations of Cel was assessed using FCM. According to Fig. 4C and D, the apoptosis rate was reduced when incubating NCM460 cells with free Cel, CD-Cel, and Cel/NPs compared to the model group. Moreover, Cel/NPs exhibited superior cellular protective efficacy than the other two groups. Thus, Cel/NPs could substantially protect colon cells from apoptosis, which could be ascribed to the ROS-scavenging capability of Cel.

As indicated in Fig. 4E and F, CD86 and CD206 represented M1 and M2 cells, respectively. Upon treatment with LPS, the expression of CD206/CD86 in macrophages markedly decreased. Subsequently, incubating macrophages with free Cel, CD-Cel and Cel/NPs resulted in an increase in CD206/CD86 expression and Cel/NPs indicated a strongest effect. The above results revealed that Cel/NPs possessed a higher effect to inhibit M1 polarization and promote M2 polarization.

In vivo biodistribution evaluation

The ability of drugs to selectively accumulate in colon lesion tissue following oral administration is pivotal for their efficacy in treating UC. Since the mucus layer is depleted and positively charged proteins are accumulated, the inflamed colonic mucosa has a positive charge, which can provide a targeted anchor for negatively charged drug carriers [35]. Therefore, we speculated that the Cel/NPs probably enter the stomach first, and subsequently travel to the small intestine following oral administration. Due to the polysaccharide properties of CD, Cel/NPs can resist the strongly acidic pH of the stomach and the weakly acidic pH of the small intestine. Next, Cel/NPs enter the colon, and their negative charges are attracted to the positively charged surface of the ulcer. Finally, in the pathological conditions of UC characterized by enzymatic activity and a ROS-enriched environment, Cel was efficiently released. In accordance with relevant research, IVIS imaging was utilized to assess the distribution of Cel/NPs in mice induced with DSS. An in vivo imaging system recorded fluorescence images at designated times after oral administration. Figure 5A and B illustrate that after 3–6 h of oral administration, there is an inapparent distinction between all groups in

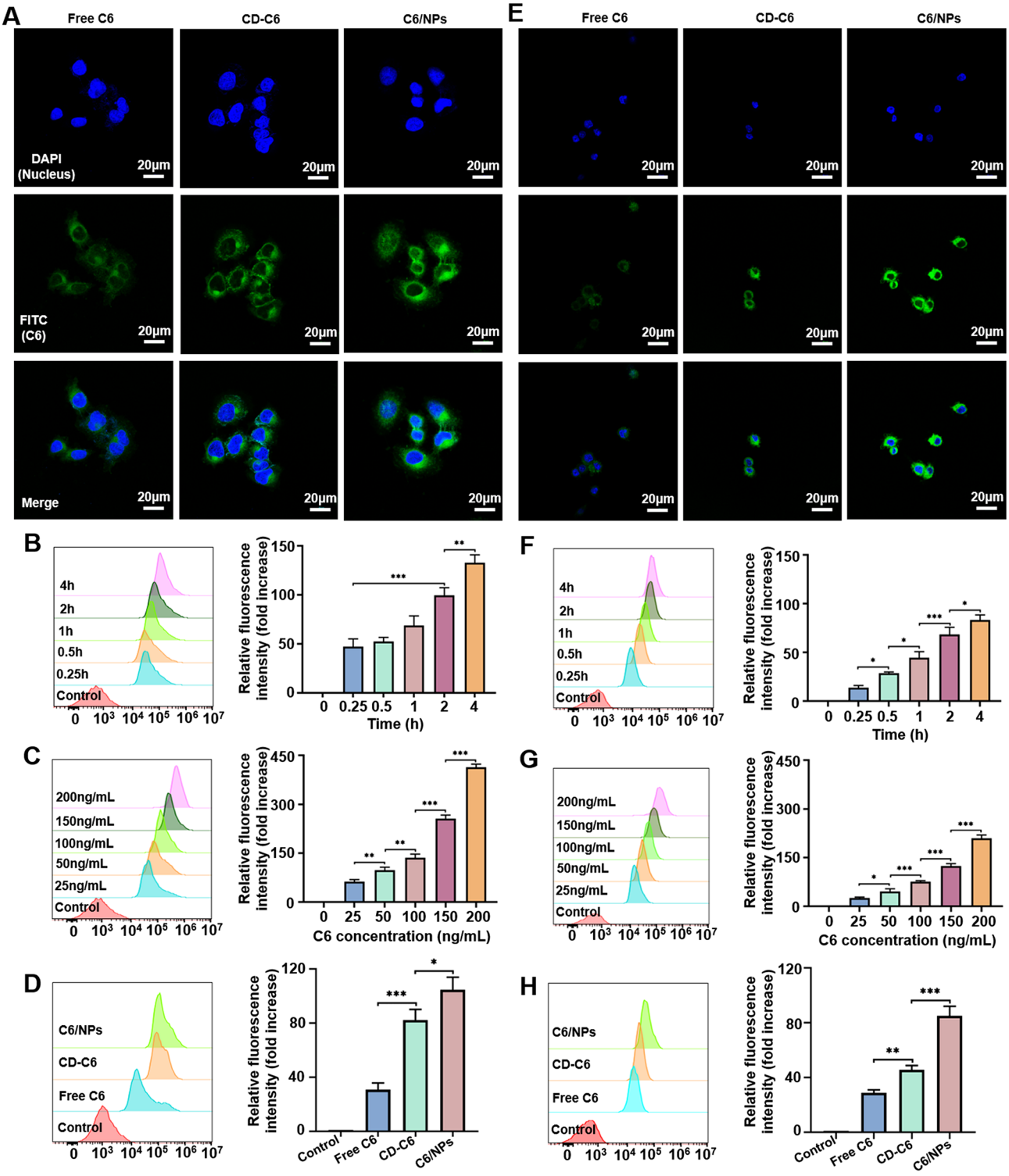

Fig. 3 Cellular uptake profiles of C6/NPs in vitro. Qualitative analysis of cellular uptake by NCM460 (**A**) and Raw264.7 (**E**) cells. Quantitative analysis of C6/NPs (with C6 concentrations of 100 ng/mL) uptake by NCM460 cells (**B**) or Raw264.7 cells (**F**) for 0.25, 0.5, 1, 2 and 4 h. Quantitative measurement of C6/NPs (with different C6 concentrations of 25, 50, 100, 150 and 200 ng/mL) uptake by NCM460 cells (**C**) or Raw264.7 cells (**G**) for 4 h. Quantitative measurement of free C6, CD-C6, and C6/NPs (C6 content is 100 ng/mL) uptake by NCM460 cells (**D**) or Raw264.7 cells (**H**) for 4 h. Data are shown as mean ± SD ($n = 3$). *$p < 0.05$, **$p < 0.01$, ***$p < 0.001$

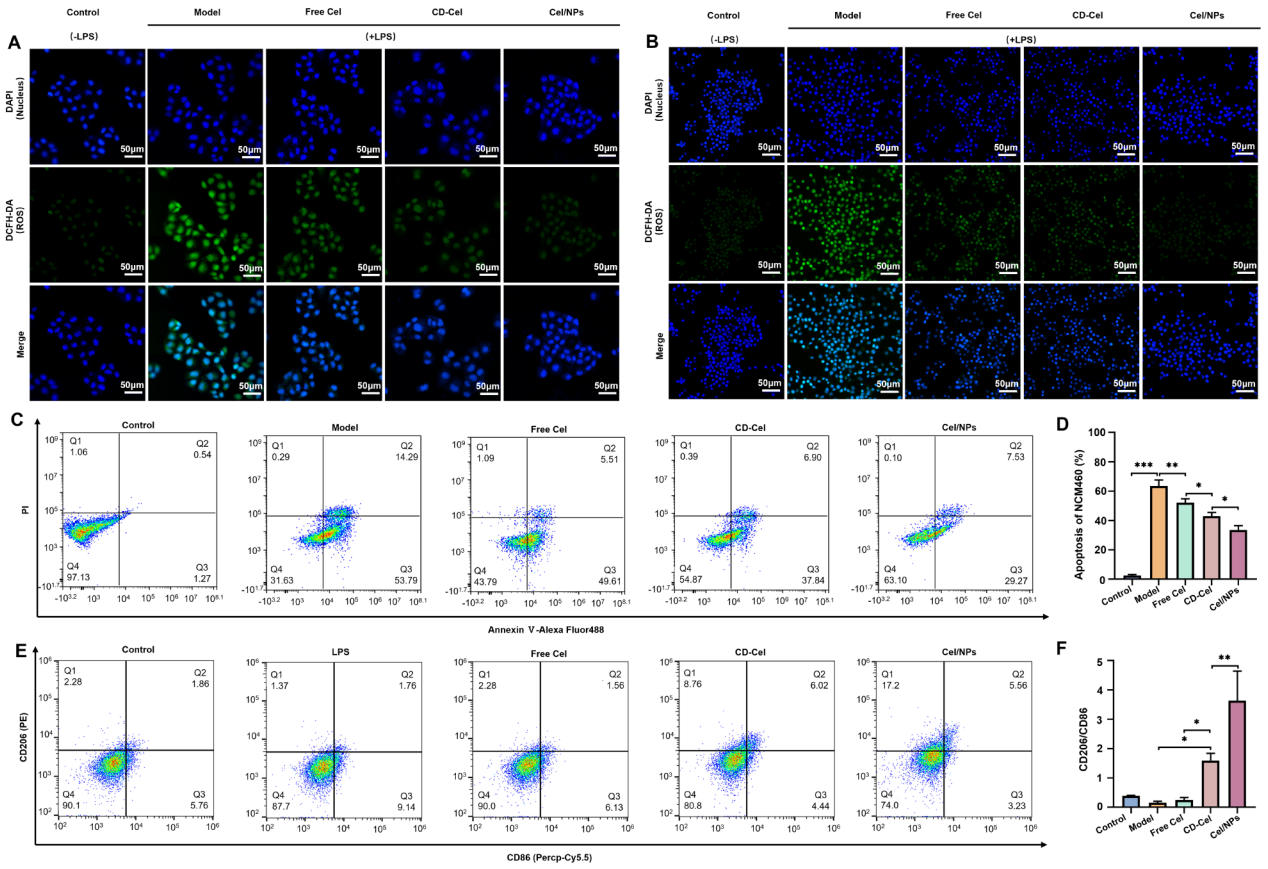

Fig. 4 In vitro cell-protective activities of Cel/NPs. Representative images of intracellular ROS of LPS-stimulated NCM460 cells (**A**) and Raw264.7 cells (**B**) after incubated with free Cel, CD-Cel and Cel/NPs for 24 h. Apoptosis determination via Annexin V-Alexa Fluor488/PI assay by FCM (**C**) and the corresponding quantitative analysis (**D**). The percentage of CD86 and CD206 were measured by FCM (**E**) and the quantitative analysis of the ratio of M2:M1 (**F**). Data are shown as mean ± SD ($n = 3$). *$p < 0.05$, **$p < 0.01$, ***$p < 0.001$

mean fluorescence intensity. Nonetheless, following oral administration for 12 h, the average fluorescence intensity of the DiR/NPs attains the strongest level ($p < 0.001$), compared to CD-DiR and free DiR. Furthermore, strong fluorescence levels persisted until 24 h. Thus, the changes in whole-body fluorescence in mice meant that PAPE-SA-CD could prolong drug retention in vivo. Subsequently, the colons of the mice were photographed 24 h after euthanasia. The results are indicated in Fig. 5C and D. According to obtaining fluorescence images and histograms, DiR/NPs exhibit a higher fluorescence intensity in the colon compared to CD-DiR or free DiR ($p < 0.001$). It has been demonstrated that DiR/NPs extend the drug's residence time in colitis tissue, delay its clearance from the body, and consequently enhance the drug's bioavailability.

Further to evaluate the absorption and distribution of Cel/NPs in UC mice, we stained the colonic tissue frozen section with DAPI. Figure 5E shows the results. Compared to free C6, both CD-C6 and C6/NPs displayed a more intense green fluorescent signal, suggesting an enhanced accumulation of the drug in colon tissue. Moreover, C6/NPs showed stronger green fluorescence than CD-C6, implying that the encapsulation ability of PAPE-SA-CD was superior to CD. Consequently, these results revealed that Cel/NPs could triumphantly deliver Cel to the colonic inflammatory site and attain effective Cel accumulation.

In vivo therapeutic effect

Therapeutic efficacy

Additionally, Cel/NPs were evaluated in vivo with DSS-induced UC models [36]. Figure 6A illustrates the process of animal model and administration. UC is distinguished by colon shortening and weight loss. Based on Fig. 6B, the body weight of mice in the model group significantly decreased from the fifth day onwards in comparison to the control group, and by the end of the experiment, the body weight of the mice had decreased to 78%. By contrast, regarding the body weight change, oral administration of different Cel preparations did not cause significant body weight loss. Moreover, as indicated in Fig. 6C, the DAI score of the CD-Cel and Cel/NPs was lower than that in the free Cel group and was

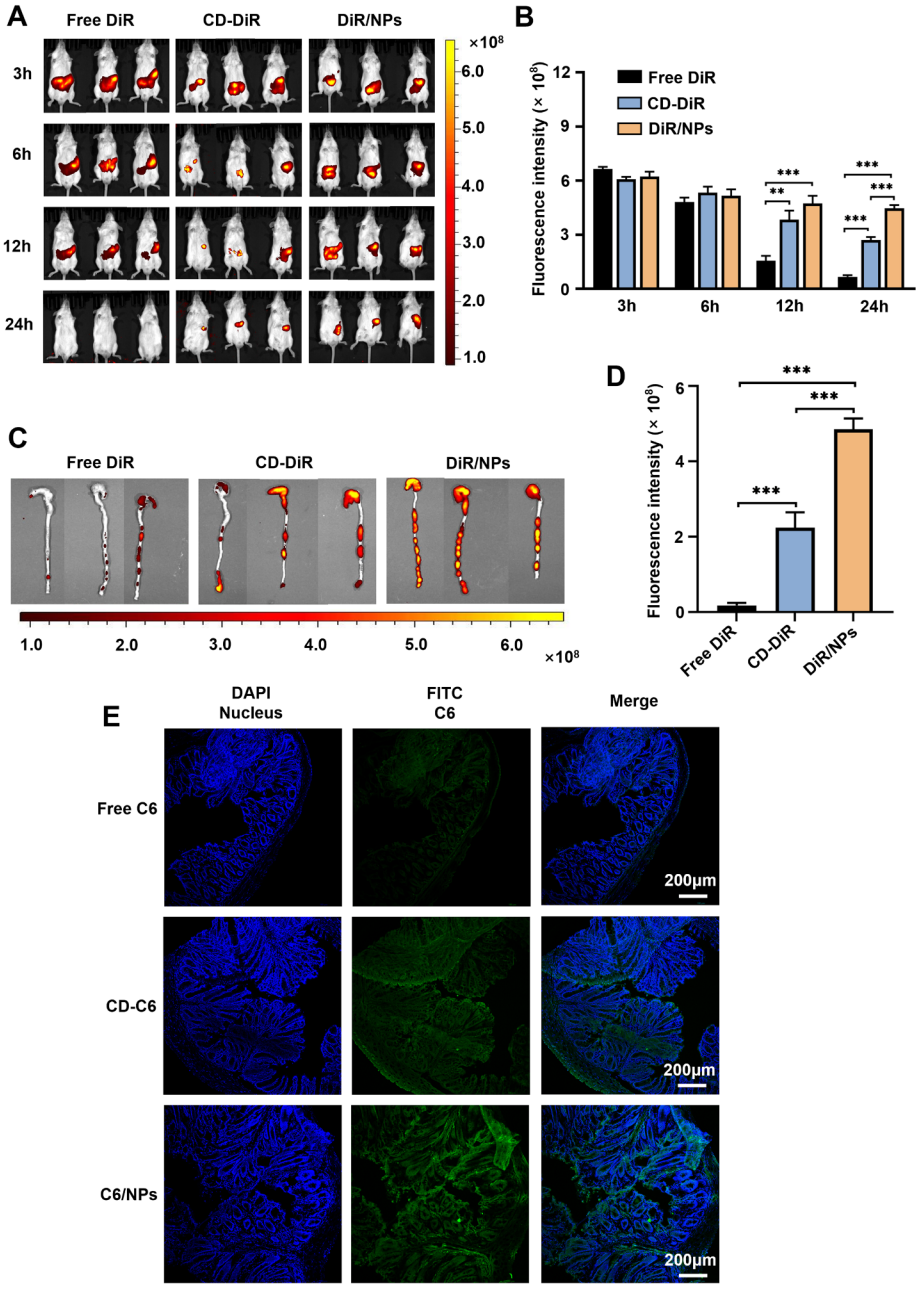

Fig. 5 The retention and colon-specific accumulation of Cel/NPs in vivo. (**A**) Fluorescence images of mice after oral delivery of free DiR, CD-DiR and DiR/NPs at 3, 6, 12 and 24 h. (**B**) Histogram of fluorescence intensity of mice. (**C**) Fluorescence images of the colon after oral delivery of free DiR, CD-DiR and DiR/NPs at 24 h. (**D**) Histogram of fluorescence intensity in colon. (**E**) Fluorescence images in colon frozen sections. Data are mean ± SD ($n = 3$). *$p < 0.05$, **$p < 0.01$, ***$p < 0.001$

dramatically lower than in the model group ($p < 0.001$) on the final day. Compared to the CD-Cel group, the DAI score of Cel/NPs was lower, which indicating Cel/NPs exhibit a more pronounced anti-UC effect. Similar disparities in colon length are evident in Fig. 6D, E, indicating that the deterioration of colon atrophy in the model group. Following drug intervention, free Cel, CD-Cel and Cel/NPs relieved the deterioration of the ulcer. Moreover, the colon images in the Cel/NPs group closely resembled those of healthy mice, suggesting that Cel/NPs effectively prevented the progression of colon atrophy induced by DSS-induced inflammation. In addition, a significantly longer colon was found in Cel/NPs than in the model, free Cel and CD-Cel groups (Fig. 6E). Furthermore, due to the fact that the spleen is a crucial immune organ, an increase in spleen weight can serve as a marker

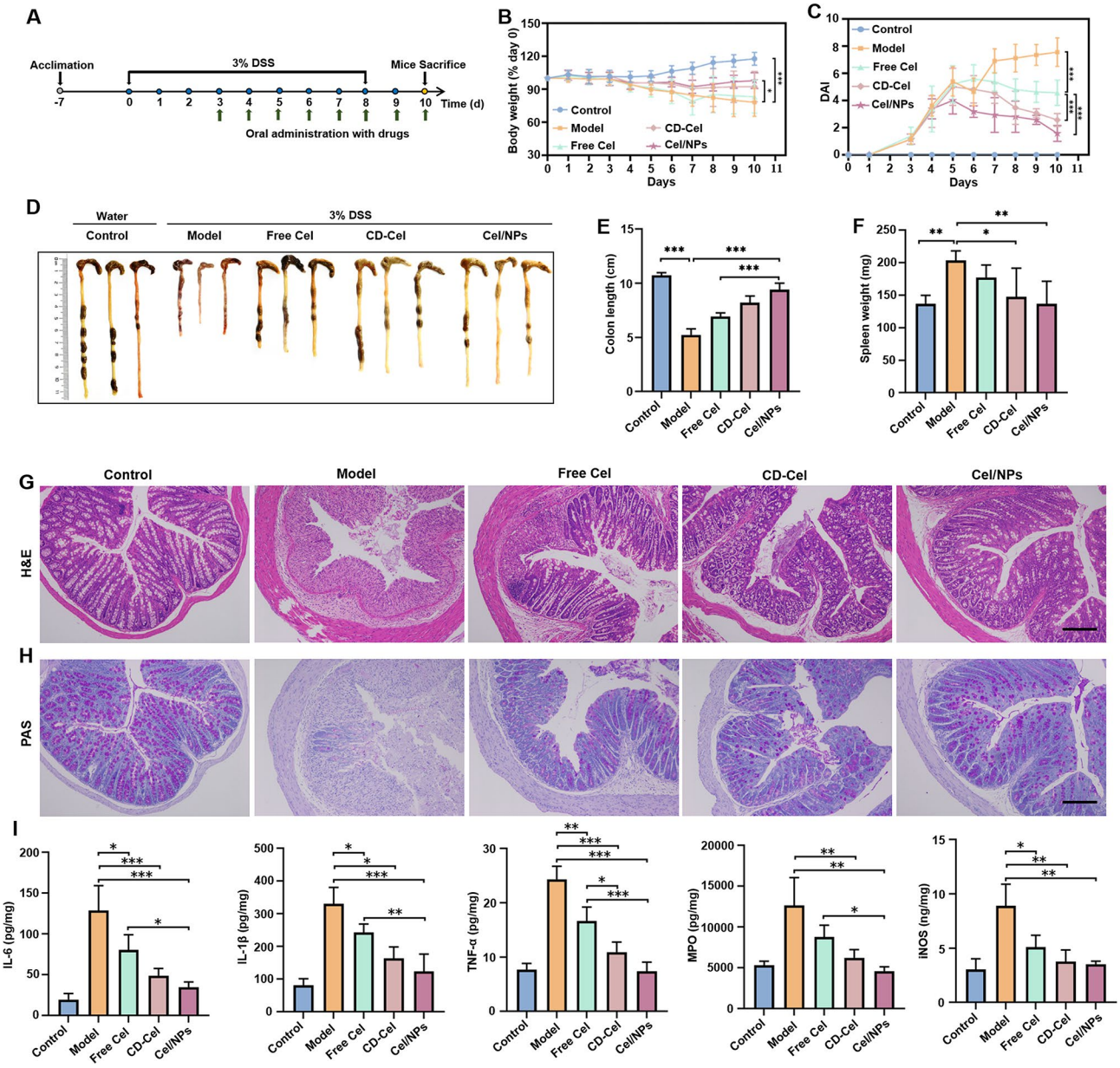

Fig. 6 The therapeutic efficacy evaluation in DSS-induced colitis. (**A**) ICR mice were used as the research objects to build a DSS-induced UC model and treatment plan. (**B**) Body weight changing with time after intervening different formulas. (**C**) DAI scores changing with time after intervening different formulas. (**D**) Image of colons isolated from mice. (**E**) Average lengths of colons. (**F**) Average spleen weight. (**G**) Images of H&E-stained histological sections (the scale bar = 200 μm). (**H**) Images of PAS-stained histological sections (the scale bar = 200 μm). (**I**) The level of IL-6, IL-1β, TNF-α, MPO and iNOS in colonic tissues isolated from different groups. Data are mean ± SD ($n = 6$). *$p < 0.05$, **$p < 0.01$, ***$p < 0.001$

of the severity of inflammation. Except for that, Fig. 6F indicates the result of the average spleen weight, which reveals that the average spleen weight of Cel/NPs group is comparable to that of the healthy mice and lighter than that of the other groups. This indicates that Cel/NPs have the ability to mitigate inflammation.

Moreover, H&E staining was employed to evaluate the pathological changes in colon tissue following drug intervention (Fig. 6G). The model group demonstrated significant infiltration of inflammatory cells in colon tissue, destruction of crypt structures, and reduction of goblet cells. It is essential to note that Cel/NPs group protect crypt structure of colon while decreasing granulocyte infiltration and edema. There is evidence supporting the effectiveness of Cel/NPs in treating colitis in mice. Additionally, according to PAS staining of colonic mucus goblet cells, there are goblet cells in the crypt of the control group. In contrast, nearly all goblet cells in the model group exhibited severe damage (Fig. 6H). Treatment with free Cel, CD-Cel, Cel/NPs could relieve the damage to

goblet cells in the colon, as well as Cel/NPs demonstrated the most favorable outcome in preserving goblet cells. The staining of PAS and H&E reveals a high degree of consistency.

Effect of Cel/NPs on anti-inflammation via inhibiting the TLR4/NF-κB signaling pathway

The severity of UC is closely correlated with the levels of inflammatory cytokines (e.g., IL-β, iNOS, TNF-α, IL-6) [37, 38]. Consequently, we assessed the levels of pro-inflammatory cytokines in the colons of mice to ascertain the therapeutic efficacy of Cel/NPs. As indicated in Fig. 6I, compared to the control group, there was a substantial increase in the the levels of serum myeloperoxidase (MPO) and the expression of pro-inflammatory factors including IL-6, TNF-α, IL-1β, and iNOS in model group. In contrast, following given with distinct preparations (free Cel, CD-Cel, Cel/NPs), the levels of MPO, IL-6, TNF-α, IL-1β, and iNOS have reduced. To our surprise, treatment with Cel/NPs demonstrated superior effectiveness in reducing the levels of MPO, IL-6, TNF-α, IL-1β, and iNOS compared to other groups. In summary, the accumulation of pro-inflammatory cytokines can be effectively suppressed by Cel/NPs.

As a classical pathway, the TLR4 signaling pathway consists of a series of proteins and cytokines, which mediate inflammatory responses and play an essential role in the pathogenesis of UC [39, 40]. As reported previously, the anti-inflammatory effect of Cel on DSS-induced UC mice was related to inhibiting the TLR4/NF-κB signaling pathway [15]. Hence, we attempted to further research the effects of Cel/NPs on typical proteins (e.g., TLR4, MyD88, and NF-κB) through immunohistochemistry. As demonstrated in Fig. 7A, B, C, D, compared to the control group, the protein level of TLR4, MyD88, and NF-κB p65 in the colon tissue of the model group was significantly increased. Following drug treatment, the expression of TLR4, MyD88, and NF-κB p65 was considerably lower compared to the model group. Interestingly, the Cel/NPs group exhibited lower expression of these three proteins than that of the free Cel and CD-Cel group. Consequently, Cel/NPs have an effective anti-inflammatory effect by inhibiting the TLR4/NF-κB signaling pathway.

The colonic barrier protection of Cel/NPs

As a result of the intestinal mucosa, harmful substances including intestinal bacteria and toxins are prevented from entering other tissues or blood circulation. Moreover, the disruption of intestinal barrier function can result in colitis. Besides, the regulation of intestinal permeability is primarily conducted by tight junctions and adhesins [41]. ZO-1 and occludin are two representative proteins that connect to cytoskeletal proteins and the tight junction and the adhesion junction, respectively [42]. They are associated with intestinal barrier function. As illustrated in Fig. 7E, F, G, there was a substantial decrease in the expression of ZO-1 (red) and occludin (green) in the model group compared to the control group, indicating serious damage to the intestinal barrier. Nonetheless, Cel/NPs significantly increased the expression of ZO-1 and occluding when compared to free Cel and CD-Cel ($p<0.001$), suggesting the protective effect of Cel/NPs on the intestinal barrier of UC mice.

Modulation of the gut microbiome by Cel/NPs in DSS-induced colitis

IBD pathogenesis is closely implicated in the dysbiosis of gut commensal microbiota [43]. To explore the influence of the gut microbiome during treatment, we examined whether Cel/NPs intervention could modulate the gut commensal microflora in DSS-colitis mice. The 16 S rRNA gene sequencing assay was employed to analyze the abundance of intestinal microbiota in fecal samples [44].

As indicated in Fig. 8A, the α diversity analysis in DSS-colitis mice was lower than in the healthy mice. Nonetheless, the Cel/NPs treatment effectively alleviated this undesirable phenomenon. Moreover, to assess the overall situation of the gastrointestinal flora, the principal coordinates analysis (PCoA) was conducted. Compared with the model group, the intestinal microbiota profile of Cel/NPs intervention was more comparable to that in the control group (Fig. 8B). Data from the common and unique intestinal flora taxa of the three groups were plotted in a Venn diagram (Fig. 8C).

Subsequently, an in-depth analysis of gut microbiota was conducted. The microbial composition at the phylum level exhibited high similarities between the control and Cel/NPs groups (Fig. 8D). Based on the statistical analysis, Cel/NPs significantly increased the proportion of Bacteroidota in the intestinal bacteria (Fig. 8E). Interestingly, in a genus level study, DSS treatment dramatically reduced the abundance of norank_f_Muribaculaceae (beneficial bacteria), whereas the Cel/NPs treatment increased in the proportion of norank_f_Muribaculaceae (Fig. 8F, G). Consequently, following Cel/NPs treatment, favorable conditions for the survival and proliferation of beneficial bacteria could be established.

For identifying the specialized microbial communities in different groups, linear discriminant analysis (LDA) effect size (LEfSe) analysis was conducted. The gut microbiota between them differed markedly. The microbiota that predominated in the DSS-colitis mice were harmful Enterobacteriaceae and Proteobacteria, among others, whereas Cel/NPs treatment resulted in a dissimilar composition compared to the model group (Fig. 8H). In brief, Cel/NPs could effectively modulate the gut commensal

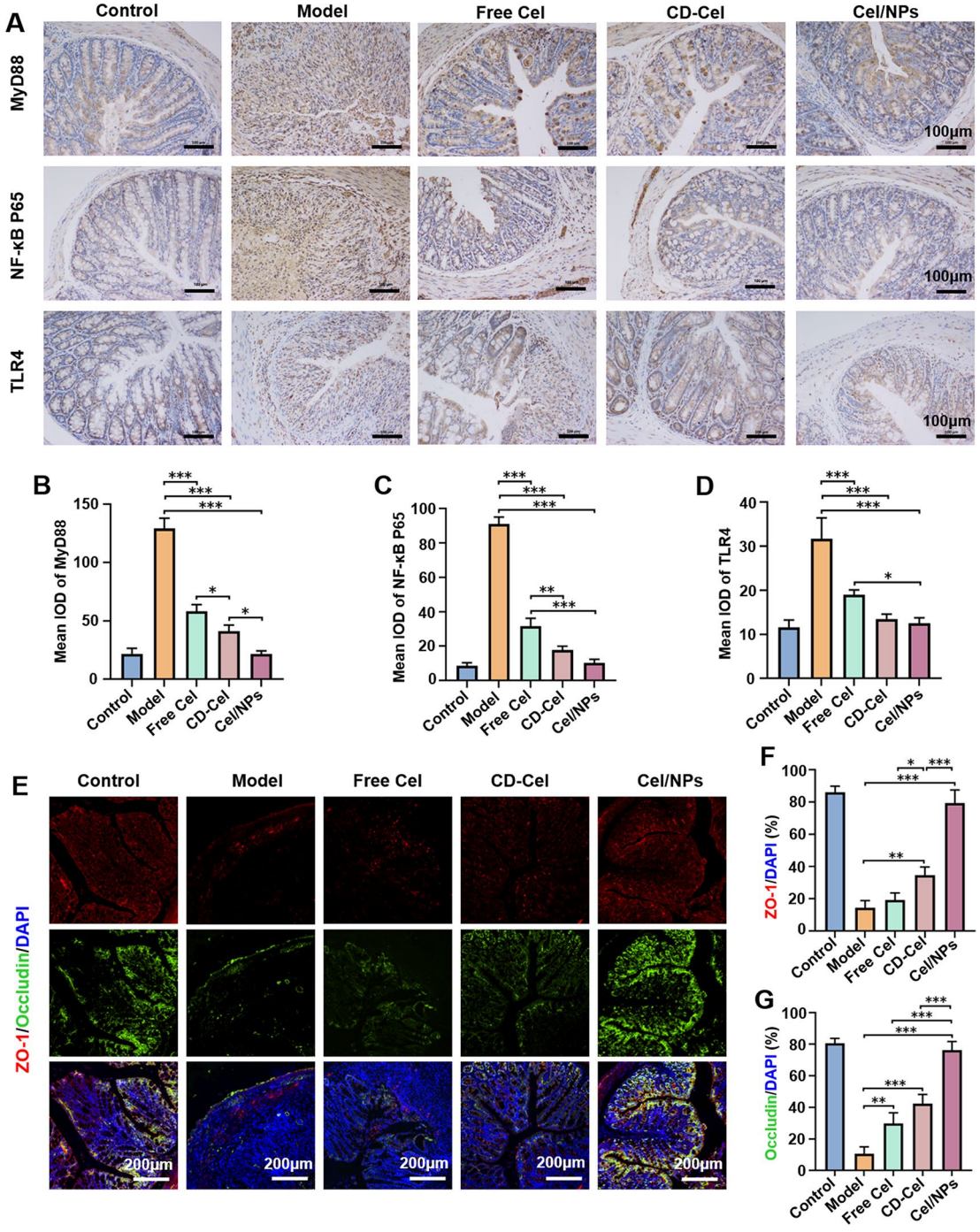

Fig. 7 Immunohistochemical (IHC) and immunofluorescence (IF) staining of colon sections of mice. (**A**) Representative IHC staining of MyD88, NF-κB p65 and TLR4 in the colon tissues (the scale bar = 100 μm). The histogram of positive of MyD88 (**B**), NF-κB p65 (**C**) and TLR4 (**D**). (**E**) The IF images of ZO-1 and occludin in colon tissues (the scale bar = 200 μm). The histogram of semi-quantitative analysis of ZO-1 (**F**) and occluding (**G**) in mouse colons. Data are mean ± SD ($n = 3$). *$p < 0.05$, **$p < 0.01$, ***$p < 0.001$

microflora to a favorable state in UC mice, which is very beneficial to the UC treatment.

Reduce hepatotoxicity after oral administration

Despite the outstanding anti-UC effects demonstrated by Cel/NPs, it remains uncertain whether any side effects would arise, given the acknowledged severe side effects of Cel. As indicated in Figure S3A, pathological evaluations of the main organ sections (heart, liver, spleen, lung, and kidneys) in UC mice were performed utilizing the H&E staining. Besides, a more extensive infiltration of inflammatory cells was evident in the liver tissue of

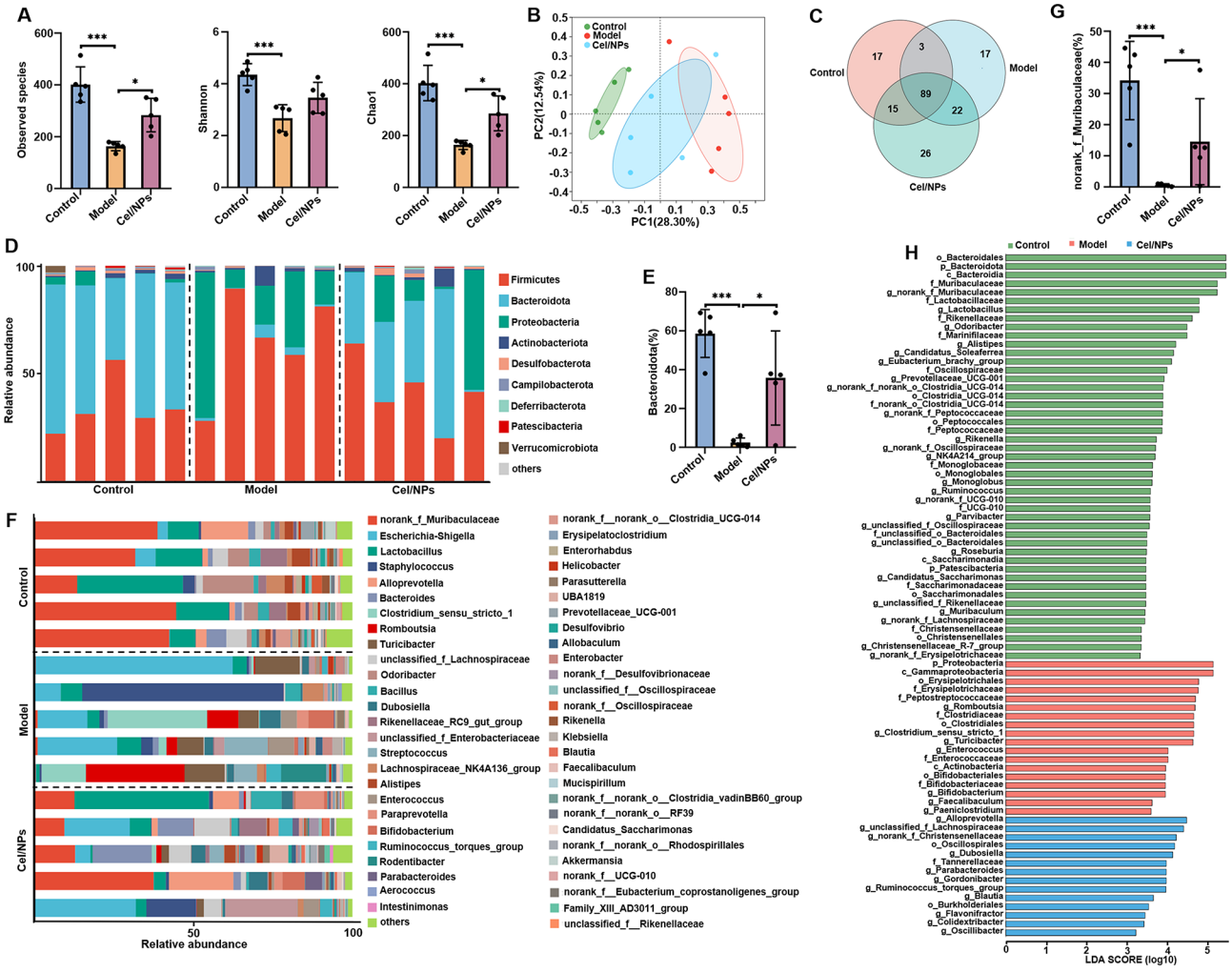

Fig. 8 Effect of Cel/NPs on intestinal flora imbalance in UC mice. (**A**) The α diversity index of observed species, Shannon and Chao1. (**B**) The PCoA analysis. (**C**) Venn diagram. (**D**) The histogram of phylum abundance among groups. (**E**) The relative abundance of Bacteroidota. (**F**) The histogram of genus abundance among groups. (**G**) The genus abundance of norank_f_Muribaculaceae. (**H**) The LEfSe analysis based on genus to phylum level. Data are mean ± SD ($n = 5$). *$p < 0.05$, **$p < 0.01$, ***$p < 0.001$

free Cel-treated mice compared with those in the control group, which suggests that free Cel led to liver damage. Interestingly, there had no obvious pathological lesions of the CD-Cel and Cel/NPs. Additionally, the analysis of physicochemical serum parameters revealed significant increases in alanine aminotransferase (ALT) levels with free Cel compared to those in the control group (Figure S3B). Conversely, Cel/NPs did not substantially affect the levels of ALT, aspirate aminotransferase (AST), urea nitrogen (BUN), or creatinine (CRE). Therefore, it can tentatively be concluded that oral administration of Cel/NPs did not exhibit any apparent toxicity.

Conclusion

In this study, based on the polysaccharide, β-CD, we designed and constructed PAPE-SA-CD-loaded Cel nanoparticles with dual enzyme/ROS sensitivity for effective treatment of DSS-induced colitis in mice. Remarkably, this nano-system offers integrated advantages, including simple preparation facilitated by the amphiphilic nature of the obtained PAPE-SA-CD, high Cel loading efficacy through the combination of CD cavity with the hydrophobic core of PAPE-SA-CD, excellent UC colon-targeting ability attributed to its negatively charged properties, and precise and burst drug release behavior due to the dual enzyme/ROS sensitivity of PAPE-SA-CD. Essentially, the pharmacodynamic experiment demonstrated that Cel/NPs successfully inhibited the progression of UC. Besides, the predominant mechanisms included regulating inflammatory factors, inhibiting the TLR4/NF-κB-mediated inflammatory pathway, scavenging the excess ROS, polarizing macrophages from M1 to M2, protecting the normal structure of the intestinal barrier, redressing the dysbiosis of the gut microbiota.

Overall, it appears that these novel nanoplatforms with versatile pharmacological functions can be employed as an effective tool for UC therapy via the oral route.

The distinctive physiological environment and challenging nature of UC often necessitate the prolonged administration of non-targeted drugs via oral or injection routes, leading to potential adverse treatment effects [45]. Our innovative nano platform aims to offer additional therapeutic options for mild-to-moderate UC patients who do not respond well to conventional medications.

However, for Cel/NPs to advance toward clinical application, thorough consideration must be given to the similarities and disparities between human and animal models, encompassing the etiology of UC, pathological alterations, disease progression, and dosage regimen, among other factors. This presents a substantial challenge, yet it is anticipated that through persistent efforts, Cel/NPs will emerge as novel alternative therapeutics, demonstrating notable efficacy and minimal side effects.

Supplementary Information

The online version contains supplementary material available at https://doi.org/10.1186/s12951-024-02725-9.

Supplementary Material 1

Acknowledgements
Not applicable.

Author contributions
Jinfeng Shi: Conceptualization, Software, Investigation, Writing-original draft preparation, Writing-review and editing. Jiahui Zhou: Conceptualization, Software, Writing-original draft preparation, Writing-review and editing. Bo Liu: Validation, Investigation, Formal analysis. Kezhou Lin: Conceptualization, Software, Methodology. Xingliang Xie: Conceptualization, Software. Xue Han: Writing-review and editing. Yanmei Sheng: Writing-review and editing. Yihan Liu: Conceptualization, Writing-review and editing. Congjian He: Methodology, Data curation, Formal analysis. Yujin Zhou: Software, Writing-original draft preparation. Nan Zhu: Conceptualization, Software, Investigation. Qian Yang: Investigation, Writing-original draft preparation. Ruifeng Luo: Conceptualization, Resources, Writing-original draft preparation, Writing-review and editing, Supervision, Project administration, Funding acquisition. Yi Li: Conceptualization, Visualization, Writing-original draft preparation, Writing-review and editing.

Funding
This work was supported by National Natural Science Foundation of China (No. 82304731), Natural Science Foundation of Sichuan Province (No. 2023NSFSC1784), Key Research and Development Program of Sichuan Province (No. 2020YFN0028), Disciplinary Construction Innovation Team Foundation of Chengdu Medical College (No. CMC-XK-2104) and Foundation of Chengdu Medical College (No. CYZZD21-02).

Data availability
Not applicable.

Declarations

Ethics approval and consent to participate
All experimental procedures were approved and reviewed by the Institutional Animal Care and Use Committee of Chengdu Medical College.

Consent for publication
All authors approve to publish the final manuscript.

Competing interests
The authors declare no competing interests.

Author details
[1]College of Pharmacy, Chengdu Medical College, No.783 Xindu Avenue, Xindu District, Chengdu 610500, China
[2]State Key Laboratory of Quality Research in Chinese Medicine, Institute of Chinese Medical Sciences, University of Macau, Taipa, Macau SAR 999078, China

Received: 24 March 2024 / Accepted: 16 July 2024
Published online: 26 July 2024

References

1. Liu S, Cao Y, Ma L, Sun J, Ramos-Mucci L, Ma Y, Yang X, Zhu Z, Zhang J, Xiao B. Oral antimicrobial peptide-EGCG nanomedicines for synergistic treatment of ulcerative colitis. J Control Release. 2022;347:544–60.
2. Baumgart D, Le Berre C. Newer biologic and small-molecule therapies for inflammatory bowel disease. N Engl J Med. 2021;385:1302–15.
3. Chang S, Murphy M, Malter L. A review of available medical therapies to treat moderate-to-severe inflammatory bowel disease. Am J Gastroenterol. 2024;119:55–80.
4. Ungaro R, Mehandru S, Allen P, Peyrin-Biroulet L, Colombel J. Ulcerative colitis. Lancet. 2017;389:1756–70.
5. Ye N, Zhao P, Ayue S, Qi S, Ye Y, He H, Dai L, Luo R, Chang D, Gao F. Folic acid-modified lactoferrin nanoparticles coated with a laminarin layer loaded curcumin with dual-targeting for ulcerative colitis treatment. Int J Biol Macromol. 2023;232:123229.
6. Chen M, Lan H, Jin K, Chen Y. Responsive nanosystems for targeted therapy of ulcerative colitis: current practices and future perspectives. Drug Deliv. 2023;30:2219427.
7. Naeem M, Bae J, Oshi M, Kim M, Moon H, Lee B, Im E, Jung Y, Yoo J. Colon-targeted delivery of cyclosporine A using dual-functional Eudragit(®) FS30D/PLGA nanoparticles ameliorates murine experimental colitis. Int J Nanomed. 2018;13:1225–40.
8. Shi J, Li J, Xu Z, Chen L, Luo R, Zhang C, Gao F, Zhang J, Fu C. Celastrol: a review of useful strategies overcoming its limitation in anticancer application. Front Pharmacol. 2020;11:558741.
9. Li J, Hao J. Treatment of neurodegenerative diseases with bioactive components of Tripterygium Wilfordii. Am J Chin Med. 2019;47:769–85.
10. Li Z, Zhang J, Duan X, Zhao G, Zhang M. Celastrol: a promising agent fighting against cardiovascular diseases. Antioxid (Basel). 2022;11:1597.
11. Zhang S, Long F, Lin H, Wang X, Jiang G, Wang T. Regulatory roles of phytochemicals on circular RNAs in cancer and other chronic diseases. Pharmacol Res. 2021;174:105936.
12. Zhao Q, Dai M, Huang R, Duan J, Zhang T, Bao W, Zhang J, Gui S, Xia S, Dai C, et al. Parabacteroides distasonis ameliorates hepatic fibrosis potentially via modulating intestinal bile acid metabolism and hepatocyte pyroptosis in male mice. Nat Commun. 2023;14:1829.
13. Li M, Guo W, Dong Y, Wang W, Tian C, Zhang Z, Yu T, Zhou H, Gui Y, Xue K, et al. Beneficial effects of celastrol on immune balance by modulating gut microbiota in experimental ulcerative colitis mice. Genom Proteom Bioinf. 2022;20:288–303.
14. An L, Li Z, Shi L, Wang L, Wang Y, Jin L, Shuai X, Li J. Inflammation-targeted celastrol nanodrug attenuates collagen-induced arthritis through NF-κB and notch1 pathways. Nano Lett. 2020;20:7728–36.
15. Xian J, Zhong X, Gu H, Wang X, Li J, Li J, Wu Y, Zhang C, Zhang J. Colonic delivery of celastrol-loaded layer-by-layer liposomes with pectin/trimethylated Chitosan Coating to enhance its Anti-ulcerative Colitis effects. Pharmaceutics. 2021;13:2005.
16. Shaker M, Ashamallah S, Houssen M. Celastrol ameliorates murine colitis via modulating oxidative stress, inflammatory cytokines and intestinal homeostasis. Chem Biol Interact. 2014;210:26–33.
17. Wang C, Dai S, Zhao X, Zhang Y, Gong L, Fu K, Ma C, Peng C, Li Y. Celastrol as an emerging anticancer agent: current status, challenges and therapeutic strategies. Biomed Pharmacother. 2023;163:114882.

18. Xu S, Yang Q, Wang R, Tian C, Ji Y, Tan H, Zhao P, Kaplan D, Wang F, Xia Q. Genetically engineered pH-responsive silk sericin nanospheres with efficient therapeutic effect on ulcerative colitis. Acta Biomater. 2022;144:81–95.
19. Xu Y, Zhu B, Li X, Li Y, Ye X, Hu J. Glycogen-based pH and redox sensitive nanoparticles with ginsenoside rh(2) for effective treatment of ulcerative colitis. Biomaterials. 2022;280:121077.
20. Yan X, Meng L, Zhang X, Deng Z, Gao B, Zhang Y, Yang M, Ma Y, Zhang Y, Tu K, et al. Reactive oxygen species-responsive nanocarrier ameliorates murine colitis by intervening colonic innate and adaptive immune responses. Mol Ther. 2023;31:1383–401.
21. Li S, Jin M, Wu Y, Jung S, Li D, He N, Lee M. An efficient enzyme-triggered controlled release system for colon-targeted oral delivery to combat dextran sodium sulfate (DSS)-induced colitis in mice. Drug Deliv. 2021;28:1120–31.
22. Zhang Y, Wang L, Wang Z, Zhou Q, Zhou X, Zhou T, Guan Y, Liu X. Surface-anchored microbial enzyme-responsive solid lipid nanoparticles enabling colonic budesonide release for ulcerative colitis treatment. J Nanobiotechnol. 2023;21:145.
23. Ishitsuka Y, Irie T, Matsuo M. Cyclodextrins applied to the treatment of lysosomal storage disorders. Adv Drug Deliv Rev. 2022;191:114617.
24. Chen Y, Wang Y, Jin Q, Ji J. Zwitterionic pendant polymer and doxorubicin decorated β-cyclodextrin guest-host micelles for efficient drug delivery. J Control Release. 2015;213:129–30.
25. Han X, Luo R, Qi S, Wang Y, Dai L, Nie W, Lin M, He H, Ye N, Fu C, et al. Dual sensitive supramolecular curcumin nanoparticles in advanced yeast particles mediate macrophage reprogramming, ROS scavenging and inflammation resolution for ulcerative colitis treatment. J Nanobiotechnol. 2023;21:321.
26. Zhang G, Liao Q, Liu Y, Wang L, Gou H, Ke C, Huang X, Xi K, Jia X. Secondary structure-induced aggregation by hydrogen peroxide: a stimuli-triggered open/close implementation by recombination. Nanoscale. 2018;10:5503–14.
27. Shi J, Ren Y, Ma J, Luo X, Li J, Wu Y, Gu H, Fu C, Cao Z, Zhang J. Novel CD44-targeting and pH/redox-dual-stimuli-responsive core-shell nanoparticles loading triptolide combats breast cancer growth and lung metastasis. J Nanobiotechnol. 2021;19:188.
28. Qi S, Luo R, Han X, Nie W, Ye N, Fu C, Gao F. pH/ROS dual-sensitive natural polysaccharide nanoparticles enhance one stone four birds effect of rhein on ulcerative colitis. ACS Appl Mater Interfaces. 2022;14:50692–709.
29. Wang X, Gu H, Zhang H, Xian J, Li J, Fu C, Zhang C, Zhang J. Oral core-shell nanoparticles embedded in hydrogel microspheres for the efficient site-specific delivery of magnolol and enhanced antiulcerative colitis therapy. ACS Appl Mater Interfaces. 2021;13:33948–61.
30. Xu Y, Zhu B, Sun R, Li X, Wu D, Hu J. Colon-targeting angelica sinensis polysaccharide nanoparticles with dual responsiveness for alleviation of ulcerative colitis. ACS Appl Mater Interfaces. 2023;15:26298–315.
31. Meng F, Wang J, Ping Q, Yeo Y. Quantitative assessment of nanoparticle biodistribution by fluorescence imaging, revisited. ACS Nano. 2018;12:6458–68.
32. Zhou J, Li M, Chen Q, Li X, Chen L, Dong Z, Zhu W, Yang Y, Liu Z, Chen Q. Programmable probiotics modulate inflammation and gut microbiota for inflammatory bowel disease treatment after effective oral delivery. Nat Commun. 2022;13:3432.
33. Wu Y, Shi R, Wu Y, Holcroft J, Liu Z, Frasconi M, Wasielewski M, Li H, Stoddart J. Complexation of polyoxometalates with cyclodextrins. J Am Chem Soc. 2015;137:4111–8.
34. Fan W, Zhang S, Wu Y, Lu T, Liu J, Cao X, Liu S, Yan L, Shi X, Liu G, et al. Genistein-derived ROS-responsive nanoparticles relieve colitis by regulating mucosal homeostasis. ACS Appl Mater Interfaces. 2021;13:40249–66.
35. Zhang C, Zeng F, Fan Z, He Z, Tai L, Peng Q, Zhang Y, Chao Z, Jiang W, Jia L, et al. An oral polyphenol host-guest nanoparticle for targeted therapy of inflammatory bowel disease. Acta Biomater. 2023;169:422–33.
36. Chen Z, Hao W, Gao C, Zhou Y, Zhang C, Zhang J, Wang R, Wang Y, Wang S. A polyphenol-assisted IL-10 mRNA delivery system for ulcerative colitis. Acta Pharm Sin B. 2022;12:3367–82.
37. Luo R, Lin M, Fu C, Zhang J, Chen Q, Zhang C, Shi J, Pu X, Dong L, Xu H, et al. Calcium pectinate and hyaluronic acid modified lactoferrin nanoparticles loaded rhein with dual-targeting for ulcerative colitis treatment. Carbohydr Polym. 2021;263:117998.
38. Neurath M. Targeting immune cell circuits and trafficking in inflammatory bowel disease. Nat Immunol. 2019;20:970–9.
39. Ai L, Ren Y, Zhu M, Lu S, Qian Y, Chen Z, Xu A. Synbindin restrains proinflammatory macrophage activation against microbiota and mucosal inflammation during colitis. Gut. 2021;70:2261–72.
40. Burgueño J, Fritsch J, González E, Landau K, Santander A, Fernández I, Hazime H, Davies J, Santaolalla R, Phillips M, et al. Epithelial TLR4 signaling activates DUOX2 to induce microbiota-driven tumorigenesis. Gastroenterology. 2021;160:797–808.
41. Guo H, Guo H, Xie Y, Chen Y, Lu C, Yang Z, Zhu Y, Ouyang Y, Zhang Y, Wang X. Mo(3)Se(4) nanoparticle with ROS scavenging and multi-enzyme activity for the treatment of DSS-induced colitis in mice. Redox Biol. 2022;56:102441.
42. Kumar A, Priyamvada S, Ge Y, Jayawardena D, Singhal M, Anbazhagan A, Chatterjee I, Dayal A, Patel M, Zadeh K, et al. A novel role of SLC26A3 in the maintenance of intestinal epithelial barrier integrity. Gastroenterology. 2021;160:1240–55.
43. Federici S, Kredo-Russo S, Valdés-Mas R, Kviatcovsky D, Weinstock E, Matiuhin Y, Silberberg Y, Atarashi K, Furuichi M, Oka A, et al. Targeted suppression of human IBD-associated gut microbiota commensals by phage consortia for treatment of intestinal inflammation. Cell. 2022;185:2879–98.
44. Chen Z, Chen Y, Hao W, Shui M, Zhang J, Zhou H, Zhang C, Wang Y, Wang S. Oral delivery of transformable bilirubin self-assembled system for targeted therapy of colitis. Adv Healthc Mater. 2023;12:2300946.
45. Zhang Y, Ma R, You C, Leng X, Wang D, Deng S, He B, Guo Z, Guan Z, Lei H, et al. Hyaluronic acid modified oral drug delivery system with mucoadhesiveness and macrophage-targeting for colitis treatment. Carbohydr Polym. 2023;313:120884.

Publisher's Note